JOURNAL OF APPLIED PHYSICS 113, 163708 (2013)

A first-principles study on the effect of biaxial strain on the ultimate performance of monolayer MoS_2-based double gate field effect transistor

Seyed Mohammad Tabatabaei,[1,a)] Maziar Noei,[1] Kaveh Khaliji,[1] Mahdi Pourfath,[1,2] and Morteza Fathipour[1]
[1]School of Electrical and Computer Engineering, University of Tehran, Tehran, Iran
[2]Institute for Microelectronics, Technische Universität Wien, Gußhausstraße 27–29/E360, A-1040 Wien, Austria

(Received 11 December 2012; accepted 9 April 2013; published online 30 April 2013)

In this work, the effect of biaxial strain on the electronic band structure of monolayers of MoS_2 is investigated. The effective mass of carriers under different strain values is extracted and the achieved results are discussed. For the first time, we have assessed the effect of biaxial strain on the ultimate performance of MoS_2-based double gate field effect transistors (DGFETs). The results indicate that by strain engineering, a significant performance improvement of MoS_2-based DGFETs can be achieved. © *2013 AIP Publishing LLC* [http://dx.doi.org/10.1063/1.4803032]

I. INTRODUCTION

The successful experimental isolation of graphene in 2004 marks a milestone in research on ultrathin two-dimensional crystals.[1] Observation of outstanding optical and electronic properties arising from the inherent carrier confinement in these low-dimensional structures has attracted a huge attention from the scientific community to explore their potential for post-silicon nanoelectronic devices.[2–4] In this respect, although graphene possesses fascinating physical properties,[5,6] the absence of a bandgap in this material restricts its application in electronics. Therefore, various techniques for opening a bandgap in graphene have been proposed.[7–9] However, these methods not only tend to deteriorate the excellent properties of graphene they also introduce additional challenges in the fabrication process.[10]

Layered transition-metal dichalcogenides (TMDCs) represent a class of materials with strong in-plane bonding and weak out-of-plane interactions, enabling cleavage into two-dimensional sheets of atomic thickness. Contrary to graphene, TMDCs possess sizable indirect bandgaps that change to direct in monolayers, allowing prospective applications such as transistors and optoelectronic devices.[11] Particularly, single-layer molybdenum disulfide (MoS_2), a member of TMDCs family, offers a large direct experimental bandgap around 1.8 eV.[12] Figure 1 depicts the covalently bonded S-Mo-S unit cells of MoS_2 arranged in a hexagonal lattice. The neighboring planes in bulk MoS_2 are held together by weak van der Waals forces, making it possible to produce monolayers of MoS_2 using the well-established micromechanical cleavage and liquid exfoliation techniques.[13]

Despite having a noticeable direct bandgap at high-symmetry K point (see Fig. 2), due to the very low mobility in monolayer MoS_2 ($\sim 0.5-3\,\mathrm{cm^2V^{-1}s^{-1}}$),[13] this material did not receive much attention from a semiconductor device perspective until very recently when a high-performance field effect transistor (FET) with MoS_2 as its channel material has been realized.[14] The large enhancement in the field effect mobility of monolayer MoS_2 in this realization ($\sim 200\,\mathrm{cm^2V^{-1}s^{-1}}$) is attributed to the Coulomb screening by the high-κ HfO_2 dielectric.[15] Moreover, an excellent room-temperature I_{on}/I_{off} ratio exceeding 10^8 and a steep subthreshold slope of 74 mV/decade in this work indicate the usefulness of this material for digital applications where ultra-low standby power consumption is required.[14]

Strain engineering is shown to be an effective method for boosting device performance in CMOS technology.[16] Furthermore, strain is ubiquitous in stretchable electronics applications where ultrathin two-dimensional materials are highly expected to bear fruit.[17] Therefore, evaluating the effect of strain on the electronic band structure and transport properties of monolayer MoS_2 is appealing from both scientific and technological viewpoints.

The effect of strain on the electronic band structure of MoS_2 is studied in Refs. 18–23. According to these works, a large enough biaxial strain component can cause a semiconductor-metal transition in MoS_2 monolayers. Additionally, strain alters the effective mass of carriers and changes the direct bandgap of monolayer MoS_2 to an indirect one. However, no previous investigation is performed on the performance of MoS_2-based FETs under strain. In this work,

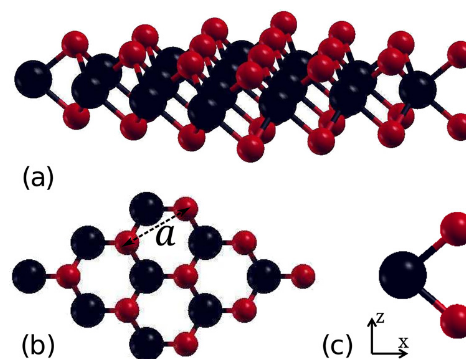

FIG. 1. (a) Side and (b) top views of the atomistic configuration of a monolayer of MoS_2. *a* denotes the lattice constant. (c) 3-atom unit cell of monolayer MoS_2. Two sulphur atoms are shown in red and one molybdenum atom is shown in black.

a)s.m.tabatabaei@ut.ac.ir

 © 2013 AIP Publishing LLC

Downloaded 02 May 2013 to 10.0.106.117. This article is copyrighted as indicated in the abstract. Reuse of AIP content is subject to the terms at: http://jap.aip.org/about/rights_and_permissions

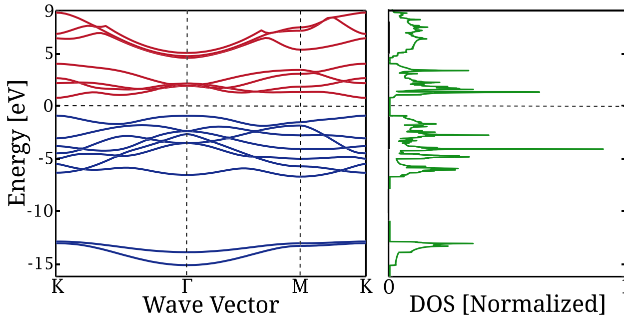

FIG. 2. The calculated electronic band structure of MoS_2 (left) in its completely relaxed structure and the corresponding density of states (right) employing the GGA method. MoS_2 is a direct semiconductor with its bandgap at the high-symmetry K point. The Fermi energy level is indicated as the line at $E = 0$ eV.

we report for the first time a theoretical study on the ultimate performance of a monolayer MoS_2-based double gate field effect transistor (DGFET) under both compressive and tensile biaxial strains. As the first step, the electronic band structure of monolayer MoS_2 under different biaxial strain values is studied, using density functional theory. After extracting the longitudinal and transverse effective masses under various strain values, the top-of-the-barrier model is employed to assess the ultimate performance limit of the DGFET.

II. APPROACH

A. First-principles calculations

In this study, the Vienna *ab initio* simulation package (VASP)[24,25] is employed for band structure calculations using the projector augmented wave formalism.[26] The Perdew-Burke-Ernzerhof[27] modification of the generalized gradient approximation (GGA) is utilized for approximating the exchange correlation potential. A cut off energy of 500 eV is adopted. A large interlayer spacing of 13 Å is used to assure the elimination of interlayer interactions which are absent in a realistic monolayer structure. A two-dimensional Γ-centered Monkhorst-Pack Brillouin-zone grid of 13 × 13 × 1 k-points is chosen for obtaining the relaxed structure and the mesh is increased to 35 × 35 × 1 for density of states (DOS) calculations. The energy convergence criterium is set to 10^{-7} eV in all iterations. Furthermore, it has been recently shown that among all TMDCs, the smallest spin-orbit splitting belongs to MoS_2, where spin-orbit coupling only weakly affects the band structure and is even zero at some special symmetry points.[28] Therefore, spin-orbit interaction is excluded from our band structure calculations.

The application of biaxial strain is modelled by straining the lattice constant to the desired value followed by a relaxation in which all the atomic positions in the unit cell are allowed to change while keeping the lattice vectors fixed. The modification in the lattice constant is achieved by changing it from a to $a + \varepsilon a$, where ε denotes the value of the applied strain. Also, compressive and tensile strains are denoted by negative and positive values of ε, respectively. Finally, the effective mass, energy gap, and the density of states are extracted at various strain values.

B. Top-of-the-barrier model

An analytical ballistic model for MOSFET is utilized here to assess the ultimate performance of monolayer MoS_2-based DGFET (see Fig. 3) both in its relaxed state and under strain.[29] In the first step, the density of states as a function of energy is evaluated from the first-principles electronic band structure. The obtained density of states is then used for calculating the non-equilibrium and equilibrium electron densities according to Eqs. (1) and (2), respectively,

$$N = \frac{1}{2}\int_{-\infty}^{+\infty} D(E) f(E - E_f) dE, \tag{1}$$

$$N_0 = N_{0S} + N_{0D}, \tag{2}$$

where

$$N_{0S/D} = \int_{-\infty}^{+\infty} D(E) f(E - E_{FS/D} + U_{SCF}) dE. \tag{3}$$

In Eq. (3), E_{FS} and E_{FD} denote the Fermi levels of the source and drain contacts, respectively, and U_{SCF} is the self-consistent potential at the top of the barrier along the channel. U_{SCF} is evaluated by solving the electrostatic equation self consistently with charge density equation using the following relation:

$$U_{SCF} = -q(\alpha_G V_G + \alpha_D V_D + \alpha_S V_S) + \frac{q^2}{C_\Sigma}\Delta N, \tag{4}$$

where C_Σ is the parallel combination of the gate, drain, and source capacitances $(C_G + C_D + C_S)$, and $\Delta N = N - N_0$. $\alpha_{G/S/D}$ represents the controllability of the self-consistent potential by the corresponding terminal and is equal to $C_{G/S/D}/C_\Sigma$. (For a well-designed DGFET, $\alpha_G \gg \alpha_D, \alpha_S$ and the potential is primarily controlled by the gate voltage.)

Once the self consistent potential is calculated, the drain-source current density can be obtained by differencing the fluxes from the source and the drain contacts. Finally, the average velocity of the injected carriers at the top of the potential barrier is given by $v_{avg} = I_{DS}/qN$.

III. ELECTRONIC BAND STRUCTURE

The calculated electronic band structure of monolayer MoS_2 and the corresponding density of states plot are

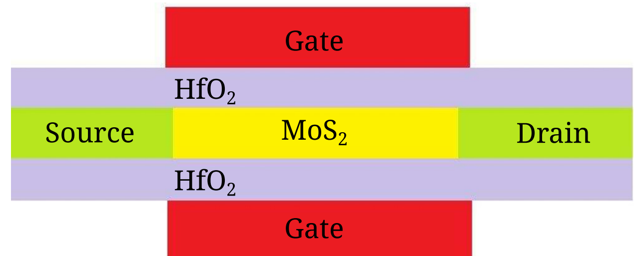

FIG. 3. Schematic of a DGFET based on 6.5 Å thick monolayer MoS_2. A 3-nm HfO_2 ($\kappa = 25$) gate dielectric and 0.6 V power supply voltage are assumed.

Downloaded 02 May 2013 to 10.0.106.117. This article is copyrighted as indicated in the abstract. Reuse of AIP content is subject to the terms at: http://jap.aip.org/about/rights_and_permissions

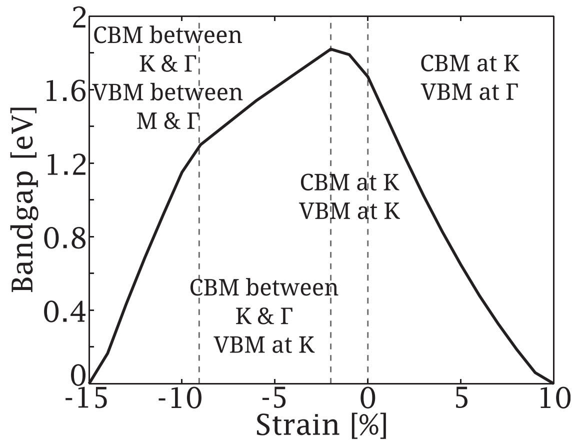

FIG. 4. The energy bandgap as a function of the applied biaxial strain.

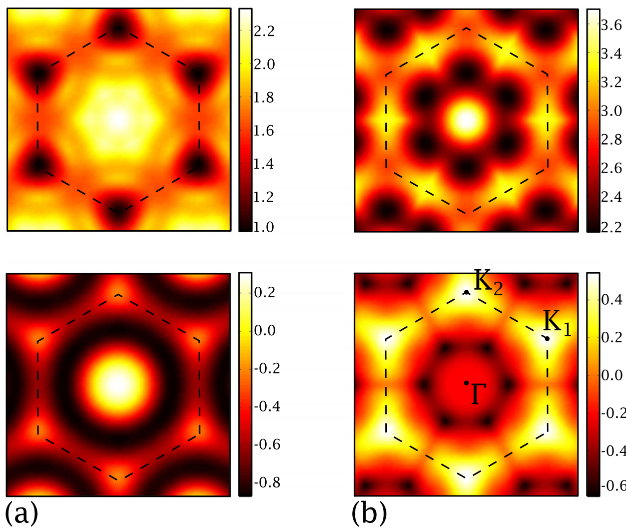

FIG. 5. The valence bands (lower figures) and the conduction bands (upper figures) under 5% tensile (a) and 5% compressive (b) strain.

shown in Fig. 2. A direct energy gap equal to 1.68 eV is evaluated at the high-symmetry K point. In order to obtain the lattice parameters, the structure is allowed to relax completely until all the forces acting on atoms become smaller than 0.001 eV/Å. Accordingly, the lattice constant, length of the covalent Mo-S bond, and vertical distance between S atoms are found to be equal to 3.18 Å, 2.41 Å, and 3.12 Å, respectively. The obtained results are in excellent agreement with previous rigorous first-principles calculations.[30–33]

Next, variations in the bandgap of monolayer MoS_2 under compressive and tensile biaxial strains as large as 15% are studied. The feasibility of the adopted range of strain values can be verified by referring to a previous first-principles study which reports 19% as the critical biaxial strain limit.[23]

Figure 4 depicts the energy bandgap as a function of the applied strain. Under tensile strain, the bandgap decreases monotonically with strain. At $\varepsilon = 10\%$, the bandgap vanishes and a semiconductor-metal transition is observed. While a relaxed monolayer MoS_2 demonstrates a direct energy gap at the K point, it becomes an indirect semiconductor under tensile strain. The indirect nature of the bandgap under tensile strain is demonstrated in Fig. 5(a), where the energies of the lowest conduction band and the highest valence band in the first Brillouin zone are plotted for $\varepsilon = 5\%$. It can be seen from this figure that the conduction band minimum (CBM) is still at the K point, while the valence band maximum (VBM) is moved to the Γ point. Hence, the valley degeneracy for both VBM and CBM is equal to two in a relaxed structure, whereas under tensile strain of 5% VBM is singly degenerate.

Under compressive strain, while the bandgap is direct for strain values smaller than 2%, it becomes indirect under larger strain values as the CBM experiences two successive moves (see Fig. 4). Additionally, under compressive strain, the energy bandgap increases first and then monotonically decreases causing a semiconductor-metal transition. Figure 5(b) shows that the valley degeneracy of both VBM and CBM is increased to six under 5% compressive strain, effectively tripling the density of states in comparison with that of a relaxed structure.

The variation of energy bandgap as a function of strain, shown in Fig. 4, can be categorized into four regions based on the curve slope. This behaviour should be attributed to the change in the atomic orbital composition of the associated crystal wavefunctions at VBM and CBM under various strain values. Investigating the details of these changes in the orbital composition of crystal wavefunctions requires further study and is beyond the scope of the current work.

Strain induces noticeable changes in the effective masses of both electrons and holes. A k-point spacing smaller than 0.03 Å^{-1} is adopted in the extraction of the effective masses to keep the parabolic effects. The longitudinal and transverse effective masses for electrons are shown in Fig. 6. It can be clearly observed that the longitudinal and transverse effective masses vary abruptly under 1% compressive strain. This abrupt change is due to the change in the CBM position. Under compressive strain smaller than 1%, CBM is located between the Γ and K points, while at larger strain values, CBM moves to the K point. Thereafter, the trend of both curves changes which, again, can be attributed to the underlying change in the contributions from different atomic orbitals to the crystal wavefunctions close to CBM.

The longitudinal and transverse effective masses for holes are shown in Fig. 7. Abrupt changes in the effective masses can be explained in a similar way to that of electrons.

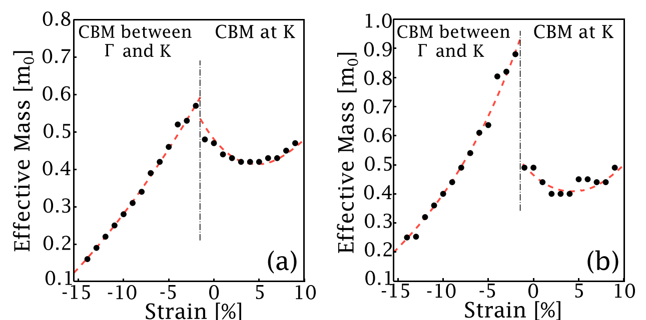

FIG. 6. (a) The longitudinal and (b) transverse effective mass of electrons along Γ–K direction.

Downloaded 02 May 2013 to 10.0.106.117. This article is copyrighted as indicated in the abstract. Reuse of AIP content is subject to the terms at: http://jap.aip.org/about/rights_and_permissions

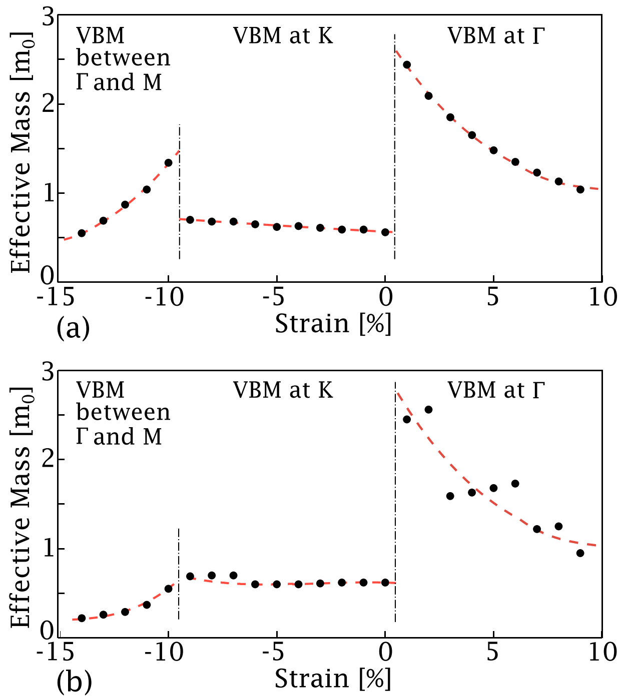

FIG. 7. (a) The longitudinal and (b) transverse effective mass of holes along Γ–K direction.

Particularly, the position of the VBM changes at two different strain values, giving rise to three distinct regions in the curves. Under compressive strain values larger than 10%, the VBM is located between Γ and M points in the first Brillouin-zone. Under smaller compressive strain values, the VBM is located at the K points. Finally, under tensile strain values, the VBM position is moved to the Γ point. Similar to the explanation given for electrons, the three different trends in the results are due to the change in the atomic orbital composition of the crystal wavefunctions in the vicinity of respective VBMs.

IV. DEVICE PERFORMANCE

The ultimate performance of the DGFET structure shown in Fig. 3 is investigated in this section under various biaxial strain values. A 3-nm HfO_2 gate dielectric is assumed. The values for α_G and α_D are chosen to be 0.880 and 0.035, respectively. The choice of these values is in accordance with the exceptional control of the gate on the ultrathin two-dimensional channel.[34] Also, it should be noted that in the ballistic regime, the current is independent of the channel length. In order to provide a fair benchmarking of the device performance under various strain values, the Fermi energy level of the source, E_F, is chosen so that an off-current density equal to 3 $\frac{\text{nA}}{\mu\text{m}}$ is obtained. Practically, E_F can be adjusted by changing the work function of the gate and the doping density in the source.

Figures 8 and 9 compare the device characteristics assuming a transport direction along the Γ–K direction and perpendicular to it, respectively. The I_{on}/I_{off} ratio and the on-current increase significantly with strain. Under a compressive strain equal to 2%, $E_F = -0.38\,\text{eV}$ and $U_{SCF} = -0.39\,\text{eV}$ while under that equal to 14%, $E_F = -0.36\,\text{eV}$ and $U_{SCF} = -0.44\,\text{eV}$. Apparently, E_F and U_{SCF} have changed in opposite directions, resulting in the increase of the on-current. It is worthwhile to notice that according to our results in Sec. III, under compressive strain smaller than 1%, the valley degeneracy of CBM is equal to six while under other strain, it is equal to two. Hence, the enhancement of the valley degeneracy under compressive strain increases the density of states and the on-state current and results in larger I_{on}/I_{off} ratio as shown in Figs. 8(c) and 9(c). Furthermore, our results predict a considerable performance improvement when the transport direction is parallel to Γ–K. This is due to the higher transverse effective mass of electrons which results in lower mobilities in the perpendicular direction.

The inset in Fig. 8(a) depicts the injection velocity of electrons at top of the barrier under various strain values and gate biases. From this figure, it is evident that the velocity of the injected carriers is increased with increasing strain due to the underlying decrease in the effective mass of electrons (see Fig. 6) which translates into a higher mobility.

Figure 10 shows the I_{on}/I_{off} ratio along the longitudinal and transverse directions, assuming holes as majority carriers. As can be seen from this figure, the improvement of I_{on}/I_{off} ratio is more pronounced along the direction normal to Γ–K. This is due to the smaller transverse effective mass of holes (see Fig. 7) which results in higher mobility in the direction perpendicular to Γ–K. Moreover, the valley degeneracy is equal to six under compressive strain values from 9% to 14%, which is three times its value at zero strain, giving rise to a three times larger density of states. Hence, a more noticeable enhancement in I_{on}/I_{off} ratio is observed for this range of applied strain. On the other hand, the smallest I_{on}/I_{off} ratio is calculated under tensile strain where VBM is at the Γ point, valley degeneracy being equal to one.

Although the presented analysis provides a useful comparison of the intrinsic characteristics of monolayer MoS_2-based DGFET under various biaxial strains, the exclusion of source/drain contacts results in highly overestimated on-currents. According to recent studies, metal contacts to MoS_2 are often accompanied by relatively high Schottky barriers.[35,36] However, the short tunneling distance in ultrathin MoS_2 which results in substantial tunneling currents has led to a general perception of an ohmic behaviour.[37]

Influence of contacts can be taken into account by modeling them as resistances ($R_{Contact}$) in series with the intrinsic resistance of the channel ($R_{Ballastic}$). Therefore, contacts degrade the performance of the DGFET by lowering the voltage drop on the intrinsic part of the device by a factor of $R_{Ballistic}/(R_{Ballistic} + 2R_{Contact})$. For the DGFET under study, the calculated ballistic resistance ranges from 0.03 to 0.43 $\Omega-\text{mm}$, while recent fabricated transistors exhibit much higher contact resistances.[35–37] Consequently, in order to harvest the full potential of MoS_2 in flexible electronics, application of more electrically transparent contacts which reduce the required bias voltage is inevitable. It is worthwhile to mention that Schottky barrier height and width are modulated by the gate voltage resulting in a variable series resistance which is larger in the off-state. Therefore, the

Downloaded 02 May 2013 to 10.0.106.117. This article is copyrighted as indicated in the abstract. Reuse of AIP content is subject to the terms at: http://jap.aip.org/about/rights_and_permissions

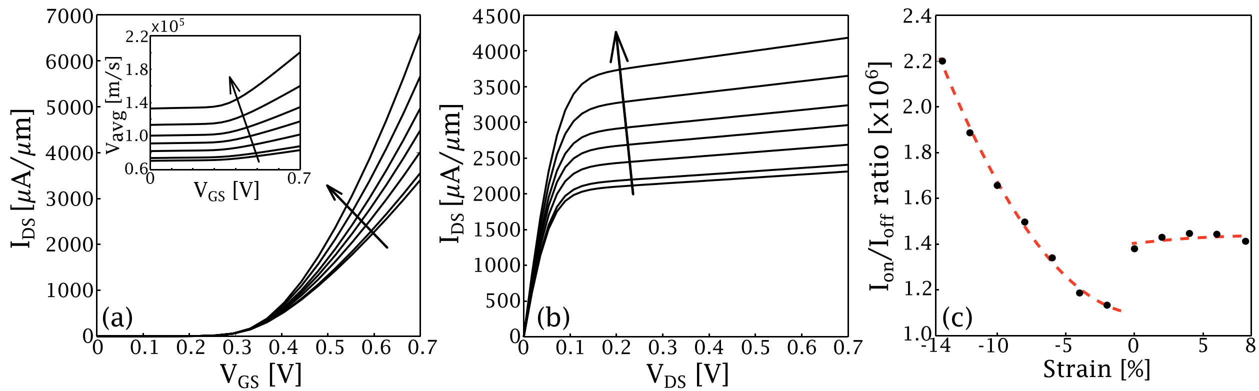

FIG. 8. (a) The transfer characteristics, (b) output characteristics, and (c) I_{on}/I_{off} ratio of the intrinsic device under various biaxial strain values. The transport direction is assumed to be along Γ–K direction and electrons are taken as the majority charge carriers. Only the results under compressive strain are shown in (a) and (b). The arrows indicate the increase of strain. Inset in (a) shows the injection velocity of electrons at top of the barrier under various strain values and gate biases.

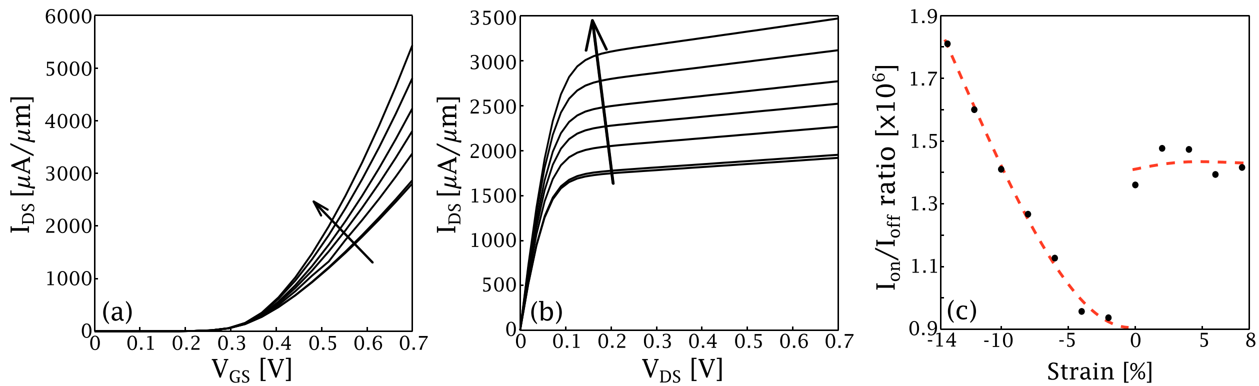

FIG. 9. (a) The transfer characteristics, (b) output characteristics, and (c) I_{on}/I_{off} ratio of the intrinsic device under various biaxial strain values. The transport direction is assumed to be normal to Γ–K direction and electrons are taken as the majority charge carriers. Only the results under compressive strain are shown in (a) and (b). The arrows indicate the increase of strain.

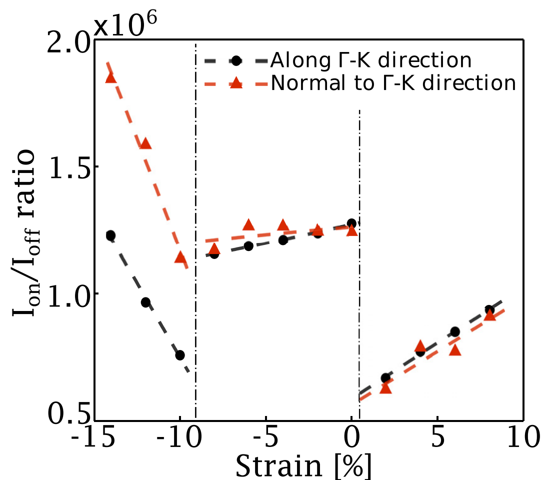

FIG. 10. The I_{on}/I_{off} ratio of the intrinsic device under different biaxial strains assuming holes as the majority charge carriers.

calculated I_{on}/I_{off} ratio will not be deteriorated in the presence of contacts.

Finally, we note that the simple ballistic model utilized here can be extended to include the effect of the floating source boundary. According to this modification, to maintain charge neutrality in the source at high gate voltage, the Fermi energy level of the source should be increased, enhancing the injection of carriers into the channel.[28] Based on our calculations, incorporating this effect will improve the on-current by at least 30% while leaving the off-current unchanged, resulting in larger I_{on}/I_{off} ratios for the intrinsic DGFET.

V. CONCLUSIONS

The effect of biaxial strain on the electronic band structure of single layer MoS_2 and the intrinsic performance of a DGFET based on this material has been investigated in this work. According to our results, strain modulates the bandgap and induces a semiconductor-metal transition. Specifically, biaxial strain closes the bandgap at 15% compressive strain and 10% tensile strain. Additionally, strain changes the nature of bandgap from direct to indirect by moving the position of VBM and CBM from that of a relaxed material, resulting in abrupt changes of the effective mass of both electrons and holes.

Strain increases the on-current of the DGFET for both n-type and p-type devices. However, the enhancement is more pronounced in p-type devices. The largest on-current compared with a relaxed structure occurs under compressive strain for both n-type and p-type devices due to the

Downloaded 02 May 2013 to 10.0.106.117. This article is copyrighted as indicated in the abstract. Reuse of AIP content is subject to the terms at: http://jap.aip.org/about/rights_and_permissions

underlying increase in the density of states. Therefore, strain engineering can be best utilized in improving the performance of p-type single layer MoS_2-based FETs.

Eventually, in order to make our study more realistic, the effect of contacts has been taken into account. Our results showed a significant lowering in the on-current upon the inclusion of the contact resistances. Hence, in order to harvest the full potential of MoS_2 in flexible electronics, application of more electrically transparent contacts is essential.

ACKNOWLEDGMENTS

The authors would like to thank Dr. Yaser Abdi and Zahra Ahangari for valuable discussions.

[1]K. S. Novoselov, A. Geim, S. Morozov, D. Jiang, Y. Zhang, S. V. Dubonos, I. V. Grigorieva, and A. A. Firsov, Science **306**, 666 (2004).
[2]F. Bonaccorso, Z. Sun, T. Hasan, and A. C. Ferrari, Nature Photon. **4**, 611 (2010).
[3]C. R. Dean, A. F. Young, I. Meric, C. Lee, L. Wang, S. Sorgenfrei, K. Watanabe, T. Taniguchi, P. Kim, K. L. Shepard, and J. Hone, Nat. Nanotechnol. **5**, 722 (2010).
[4]Z. Yin, H. Li, H. Li, L. Jiang, Y. Shi, Y. Sun, G. Lu, Q. Zhang, X. Chen, and H. Zhang, ACS Nano **6**, 74 (2012).
[5]K. I. Bolotin, K. J. Sikes, Z. Jiang, M. Klima, G. Fudenberg, J. Hone, P. Kim, and H. L. Stormer, Solid State Comm. **146**, 351 (2008).
[6]K. S. Novoselov, Z. Jiang, Y. Zhang, S. V. Morozov, H. L. Stormer, U. Zeitler, J. C. Maan, G. S. Boebinger, P. Kim, and A. K. Geim, Science **315**, 1379 (2007).
[7]X. Li, X. Wang, L. Zhang, S. Lee, and H. Dai, Science **319**, 1229 (2008).
[8]J. Bai, X. Zhong, S. Jiang, Y. Huang, and X. Duan, Nat. Nanotechnol. **5**, 190 (2010).
[9]R. Balog, B. Jorgensen, L. Nilsson, M. Andersen, E. Rienks, M. Bianchi, M. Fanetti, E. Laegsgaard, A. Baraldi, S. Lizzit, Z. Sljivancanin, F. Besenbacher, B. Hammer, T. G. Pedersen, P. Hofmann, and L. Hornekaer, Nature Mater. **9**, 315 (2010).
[10]D. R. Cooper, B. D'Anjou, N. Ghattamaneni, B. Harack, M. Hilke, A. Horth, N. Majlis, M. Massicotte, L. Vandsburger, E. Whiteway, and V. Yu, ISRN Condens. Matter Phys. **2012**, 1 (2012).
[11]Q. H. Wang, K. Kalantar-Zadeh, A. Kis, J. N. Coleman, and M. S. Strano, Nature Nanotechnol. **7**, 699 (2012).
[12]K. Mak, C. Lee, J. Hone, J. Shan, and T. F. Heinz, Phys. Rev. Lett. **105**, 136805 (2010).
[13]K. S. Novoselov, D. Jiang, F. Schedin, T. J. Booth, V. V. Khotkevich, S. V. Morozov, and A. K. Geim, Proc. Nat. Acad. Sci. **102**, 10451 (2005).
[14]B. Radisavljevic, A. Radenovic, J. Brivio, V. Giacometti, and A. Kis, Nat. Nanotechnol. **6**, 147 (2011).
[15]Y. Yoon, K. Ganapathi, and S. Salahuddin, Nano Lett. **11**, 3768 (2011).
[16]See http://www.itrs.net/ for International technology road map for semiconductors.
[17]B. Radisavljevic, M. B. Whitwick, and A. Kis, ACS Nano **5**, 9934 (2011).
[18]E. Scalise, M. Houssa, G. Pourtois, V. Afanas'ev, and A. Stesmans, Nano Res. **5**, 43 (2012).
[19]Q. Yue, J. Kang, Z. Shao, X. Zhanga, S. Changa, G. Wanga, S. Qina, and J. Li, Phys. Lett. A **376**, 1166 (2012).
[20]Y. Ding, Y. Wang, J. Ni, L. Shi, S. Shi, and W. Tang, Physica B **406**, 2254 (2011).
[21]W. S. Yun, S. Han, S. C. Hong, I. G. Kim, and J. Lee, Phys. Rev. B **85**, 033305 (2012).
[22]P. Lu, X. Wu, W. G. and X. C. Zeng, Phys. Chem. Chem. Phys. **14**, 13035 (2012).
[23]T. Li, Phys. Rev. B **85**, 235407 (2012).
[24]G. Kresse and J. Furthmüller, Phys. Rev. B **54**, 11169 (1996).
[25]G. Kresse and D. Joubert, Phys. Rev. B **59**, 1758 (1999).
[26]P. E. Blchl, Phys. Rev. B **50**, 953 (1994).
[27]J. P. Perdew, K. Burke, and M. Ernzerhof, Phys. Rev. Lett. **77**, 3865 (1996).
[28]Z. Y. Zhu, Y. C. Cheng, and U. Schwingenschlögl, Phys. Rev. B **84**, 153402 (2011).
[29]A. Rahman, S. Datta, and M. S. Lundstrom, IEEE Trans. Electron Devices **50**, 1853 (2003).
[30]Y. Li, Z. Zhou, S. Zhang, and Z. Chen, J. Am. Chem. Soc. **130**, 16739 (2008).
[31]A. R. Botello-Mendez, F. Lopez-Urias, M. Terrones, and H. Terrones, Nanotechnology **20**, 325703 (2009).
[32]S. Lebegue and O. Eriksson, Phys. Rev. B **79**, 115409 (2009).
[33]H. S. S. Ramakrishna Matte, A. Gomathi, A. K. Manna *et al.*, Angew. Chem., Int. Ed. **49**, 4059 (2010).
[34]L. Liu, S. B. Kumar, Y. Ouyang, and J. Guo, IEEE Trans. Electron Devices **58**, 3042 (2011).
[35]H. Liu, A. T. Neal, and P. D. Ye, ACS Nano **6**, 8563 (2012).
[36]S. Kim, A. Konar, W. Hwang, J. H. Lee, J. Lee, J. Yang, C. Jung, H. Kim, J. Yoo, J. Choi, Y. W. Jin, S. Y. Lee, D. Jena, W. Choi, and K. Kim, Nature Commun. **3**, 1011 (2012).
[37]S. Das, H. Y. Chen, A. V. Penumatcha, and J. Appenzeller, Nano Lett. **13**, 100 (2013).

Downloaded 02 May 2013 to 10.0.106.117. This article is copyrighted as indicated in the abstract. Reuse of AIP content is subject to the terms at: http://jap.aip.org/about/rights_and_permissions